Phys. Status Solidi A **214**, No. 10, 1700050 (2017) / **DOI** 10.1002/pssa.201700050

physica status solidi a
www.pss-a.com
applications and materials science

Controlled synthesis and photoluminescence properties of In_2O_3 rods with dodecahedron In_2O_3 microcrystals on top

Hassan Ouacha*[,1], Ali Hendaoui[2], Ulf Kleineberg[3], Hamad Albrithen[4], and Abdallah Azzeer[4]

[1] King Abdullah Institute for Nanotechnology, King Saud University, P.O. Box 2455, Riyadh 11451, Saudi Arabia
[2] Department of Physics, College of Science and General Studies, Alfaisal University, Riyadh 11533, Saudi Arabia
[3] Faculty of Physics, Ludwig Maximilian University of Munich, 85748 Garching, Germany
[4] Physics and Astronomy Department, King Saud University, Riyadh 11451, Saudi Arabia

Received 31 January 2017, revised 23 May 2017, accepted 12 June 2017
Published online 3 July 2017

Keywords 1D growth, indium oxide, optical resonator, photoluminescence, vapor-solid growth

* Corresponding author: e-mail houacha@ksu.edu.sa, Phone: +966-11-4670663, Fax: +966-11-4677317

In_2O_3 rods with dodecahedron In_2O_3 microcrystals on top were synthesized in an electrical furnace via Au-catalyzed vapor transport process. A catalyst-assisted selective vapor-solid (VS) growth was proposed to explain the formation of the dodecahedron In_2O_3 microcrystal, while the self-catalytic VS growth mechanism dominated the subsequent one-dimensional (1D) growth of the In_2O_3 rod underneath the In_2O_3 microcrystal. The structural evolution of these structures was carefully examined during the synthesis process by controlling the growth parameters. The morphologies, crystalline structures and surface chemistry were characterized by scanning electron microscopy (SEM), X-ray diffraction technique (XRD), and X-ray photoelectron spectroscopy (XPS), respectively. The photoluminescence (PL) spectrum at room temperature of the as-grown In_2O_3 structures exhibited both UV and blue luminescence emission under one excitation at 260 nm, which may be related to the existence of oxygen vacancies. The synthesized multifaceted In_2O_3 microcrystal has shown to contain a large number of vertices and may find many applications in developing three-dimensional (3D) resonators. This work will not only enrich the synthesis science but also will open doors for applications of such structures in optical devices.

1 Introduction Micro/nano-structures, such as tubes, wires, belts, and rods have attracted much interest for various potential technological applications [1–4]. For example, Indium oxide (In_2O_3), which is a well-known wide bandgap (~3.6 eV) semiconductor, has been extensively studied for advanced applications in electronic, optoelectronic, photo-detectors, memory devices, and high sensitivity sensors [5–10]. In this perspective, there has been a large number of reports on the preparation of In_2O_3 micro/nanostructures by various techniques such as thermal evaporation [11], sol–gel deposition [12], chemical vapor deposition (CVD) [13], carbothermal reduction [4, 14], and laser ablation [15]. While much attention has been paid to the fabrication of In_2O_3 micro/nanowires, investigations on other structures having different morphologies and cross-sections are still limited. Single crystalline In_2O_3 nanopyramids and nanocolumns have been synthesized by a physical evaporation method without any catalytic action and using gold as the catalyst [16]. Moreover, chains of nanopyramids connected by nanowires, forming a necklace-like structure, as well as cubes and arrow-like structures consisting of a long rod with a micron size pyramid on top have been grown by thermal treatment of InN powder [17]. Over the past years, remarkable progress has been made to correlate between the used preparation techniques and shape of In_2O_3 structures, which would be important for the understanding of the growth mechanisms. In_2O_3 nanorods with rectangular cross sections have been successfully synthesized using Au as a catalyst through CVD method [18], and a competitive growth model between axial growth under the vapor–liquid–solid (VLS) mechanism and lateral growth controlled by the vapor–solid (VS)

mechanism was proposed to explain the formation of the rectangular cross section and the size change of the In_2O_3 nanorods. Vertically aligned In_2O_3 nanowires with hexagonal and square cross-sections were grown on a-plane sapphire substrate by the method of catalyst-assisted carbothermal reduction, and the concept of supersaturation in Au catalyst was proposed to explain the formation of these two types of nanowires [19]. In_2O_3 faceted structures, such as octahedrons have been synthesized in an improved CVD system, and the formation of these structures was ascribed to VS mechanism [20]. In these reports, surface energy consideration with respect to crystallographic planes of In_2O_3 was included [18–20]. Beside the synthesis of In_2O_3 structures, intensive studies on the electronic structure and the use of In_2O_3 as a semiconductor material in novel or improved conventional devices were recently reported [21]. Bulk and surface electronic structure study carried out by King et al. [22] showed that the band gap of single-crystalline In_2O_3 was determined as 2.93 and 3.02 eV for the cubic bixbyite and rhombohedral polymorphs, respectively. This lower energy of about 3 eV can be attributed to transitions between the highest valence-band states and states at the conduction-band minimum being dipole forbidden or having only minimal dipole intensity [22]. As to the optical performance, In_2O_3 structures with faceted shape as optical resonators have attracted great attentions in recent years [23, 24]. Optical resonant modes in In_2O_3 microwire cavities with irregular hexagonal cross section have been observed in the visible spectral range [23]. In_2O_3 octahedra were studied as optical resonators and bow-tie modes were observed at room temperature by using the spatially resolved spectroscopic technique [24]. These studies indicate that In_2O_3 optical resonators may be good candidates for the development of novel cavity-based optical devices.

In general, the search for well-defined In_2O_3 structures with different morphologies and different structural shapes on the top will greatly promote this material for the development of miniature devices and fundamental physics research in the fields of electronics, optics, and optoelectronics. Moreover, there is a lack of reporting the direct evidence of the structural evolution of In_2O_3 structures during the synthesis process. In this work, we report the synthesis of In_2O_3 micro-rods with three-dimensional (3D) In_2O_3 microcrystals on top by Au-catalyzed CVD process and carefully analyze the growth mechanism of these structures by examining step-by-step the structural evolution of the structures during the synthesis process. We also report the growth of the In_2O_3 microcrystal, both as an individual structure and as a cap on top of the In_2O_3 rod by controlling the growth process. The possible mechanisms behind the room-temperature photoluminescence (PL) characteristics of our as-grown In_2O_3 structures are discussed and potential application of these structures as three-dimensional (3D) resonators is proposed. Throughout this paper, we call In_2O_3 micro-rod the full structure that consists of both In_2O_3 rod and In_2O_3 microcrystal on top.

2 Experimental

2.1 Sample preparation Dodecahedron In_2O_3 microcrystals and In_2O_3 micro-rods were synthesized by Au-catalyzed CVD process using indium (In) metal and oxygen vapor as source materials. High purity (99.995%) In metal shots were loaded into a ceramic boat and positioned at the center of a quartz tube inside a horizontal tube furnace. The furnace is equipped with a rotary vacuum pump and argon/oxygen gas mixture source. Prior to the growth, Au films with a thickness of 2 nm were deposited on quartz substrate by an electron-beam evaporator. The substrate was placed close to In metal source, mounted in a vertical position at a height of 25 mm, and facing the gas mixture flow. Before heating, the quartz tube was evacuated to a base pressure below 0.1 Pa, and then filled with argon/oxygen gas mixture ($Ar:O_2 = 9:1$) at a rate of 100 sccm. Argon was used as the carrier gas. Experiment I and experiment II were conducted to synthesize dodecahedron In_2O_3 microcrystals and In_2O_3 micro-rods, respectively. In experiment I, 0.1 g of In was used and the quartz tube was heated to 900 °C at a heating rate of 31 °C min^{-1} and kept at this temperature for different growth times (0, 5, 10, and 20 min) under the constant flow of Ar/O_2 gas mixture. During the growth, the process pressure was maintained at 168 Pa. In experiment II, In weight in the range of 0.15–4 g was used, the growth temperature was set to 1000 °C and the quartz tube was kept at this temperature for different growth times (25, 30, 40, and 120 min). Other experimental conditions were kept unchanged. When the growth temperature was chosen to be 800 °C, only In_2O_3 in a shape of islands were found. Furthermore, areas in some samples were deliberately omitted from Au and we observed that no growth occurred at any of the used growth temperature. The parameters for each experiment are summarized in Table 1. In each experiment, the synthesis process was terminated at the chosen growth time to examine the morphology evolution of the resultant structure and understand its growth mechanism. When the setting growth time was up, the furnace was turned off and cooled down to room temperature. At the end of the process, a yellow layer was observed on the quartz

Table 1 Experimental condition for experiment I and II.

experiment	structure	growth temperature	Ar/O_2 mixture	Ar/O_2 flow	pressure	in weight
I	Dodecahedron In_2O_3 microcrystal	900 °C	9:1	100 sccm	168 Pa	0.1 g
II	In_2O_3 micro-rods	1000 °C	9:1	100 sccm	168 Pa	3.8 g

substrate. The same synthesis processes were performed four times to confirm the reproducibility of the growth phenomena.

2.2 Material characterization The morphology of the product was investigated using a Field Emission Scanning Electron Microscopy (FE-SEM S-4800) operating at 15 kV. The crystalline phase identification was conducted by X-ray diffraction (XRD) system in the 2θ range from 10° to 90° at a scanning rate of 0.1° per 10 s using an X-ray diffractometer (Rigaku) with CuKα radiation ($\lambda = 1.54$ Å). The surface chemistry was examined by X-ray photoelectron spectroscopy (XPS) using PHI, 5600ci (Eden Prarie, MN) with a monochromatic aluminum X-ray source (1487 eV). PL spectrum was measured at room temperature in the range of 280–510 nm in a Spectrofluorophotometer with a Xe lamp using excitation at 260 nm (4.76 eV).

3 Results and discussion The morphologies of In_2O_3 microcrystals and In_2O_3 micro-rods as products of experiment I and experiment II, respectively, are shown in Fig. 1. At a growth temperature of 800 °C (Fig. 1a), we observed no well-defined structures but only In_2O_3 in a shape of islands. Figure 1b shows a low magnification image of the obtained In_2O_3 microcrystals in experiment I. Magnified top view SEM image of the typical structure (Fig. 1c) shows that the In_2O_3 microcrystal presents a full symmetry of the form and has twelve plane faces. Therefore, it can also be referred to as *dodecahedron In_2O_3 microcrystal*. To the best of our knowledge, this structural shape has not been reported earlier. The base diameter of the In_2O_3 microcrystal shown in Fig. 1c is found to be 2.2 μm. Figure 1d and e show low- and high-magnification SEM images of In_2O_3 micro-rods as final product in experiment II. A magnified side view image (see Fig. 1f) shows the typical structure and reveals that the micro-rod consists of both an In_2O_3 rod with a diameter of 1.8 μm and an In_2O_3 microcrystal on top. It is found that these In_2O_3 micro-rods can reach a length in a range of 10–50 μm depending on the amount of the supplied In material source.

Figure 2a and b show the XRD pattern of the obtained structures in experiment I and II. All the sharp diffraction peaks in the two samples can be indexed to a body-centered cubic (bcc) structure with lattice constant of $a = 10.10$–10.11 Å (JCPDS No. 89-4595).

In comparison with the bulk In_2O_3 powder (inset of the bottom of Fig. 2) where the intensity $I_{(222)}$ is about three times higher than $I_{(400)}$, the ratio $I_{(222)}/I_{(400)}$ known as the crystal quality parameter [25] is found to decrease for In_2O_3 sample grown at 900 °C as shown in Fig. 2a. The trend is sustained when the temperature is increased to 1000 °C, where $I_{(222)}/I_{(400)}$ is found to be around 0.38 (Fig. 2b). This result is in agreement with previous work were indium tin oxide (ITO) films annealed above 900 °C show a dominant (400) orientation [26]. Other diffraction peaks in Fig. 2a and b correspond to (211), (411), (431), (440), (622), and (662), respectively. Dominant XRD peaks of (111) and (100) were observed in In_2O_3 octahedrons [20] and In_2O_3 nanobelts [27], respectively.

The surface composition of the obtained In_2O_3 structures was verified by XPS technique. Figure 3a and b show XPS spectra for In3d and oxygen O1s from In_2O_3 microcrystals and In_2O_3 micro-rods. The In3d core level shape and peak positions (445 and 452.5 eV for $In3d_{5/2}$ and $3d_{3/2}$, respectively) are found to be consistent with those of In_2O_3 [28].

The O1s peak displays a contribution at binding energy ranging from 529.5 to 533.5 eV with a peak position at 530.75 eV, which can be assigned to the lattice oxygen in crystalline In_2O_3 [29, 30]. However, the gold Au4f core level was not evident and no Au was detected in all the samples,

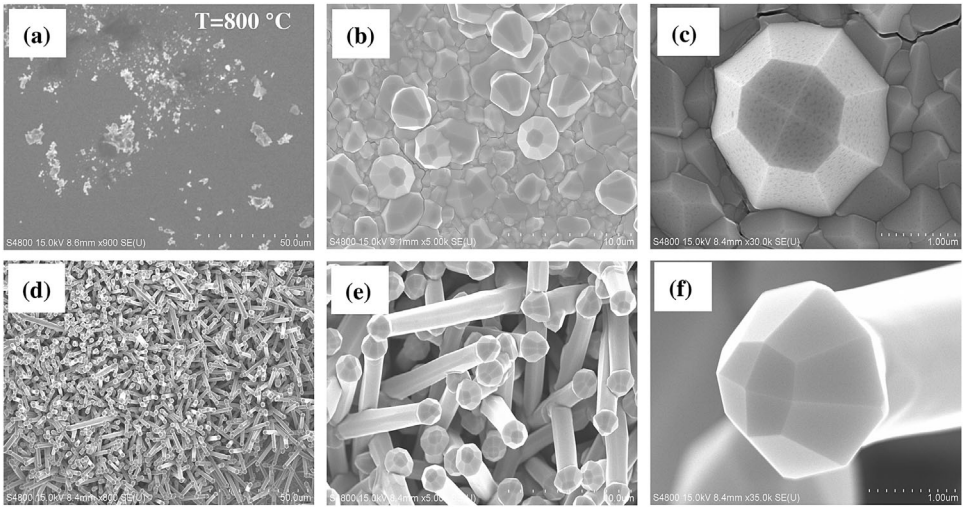

Figure 1 (a) In_2O_3 island-like shape structures obtained at 800 °C; (b, c) Low- and high-magnification SEM images of In_2O_3 microcrystals found in experiment I; (d–f) low- and high-magnification SEM images of In_2O_3 micro-rods found in experiment II.

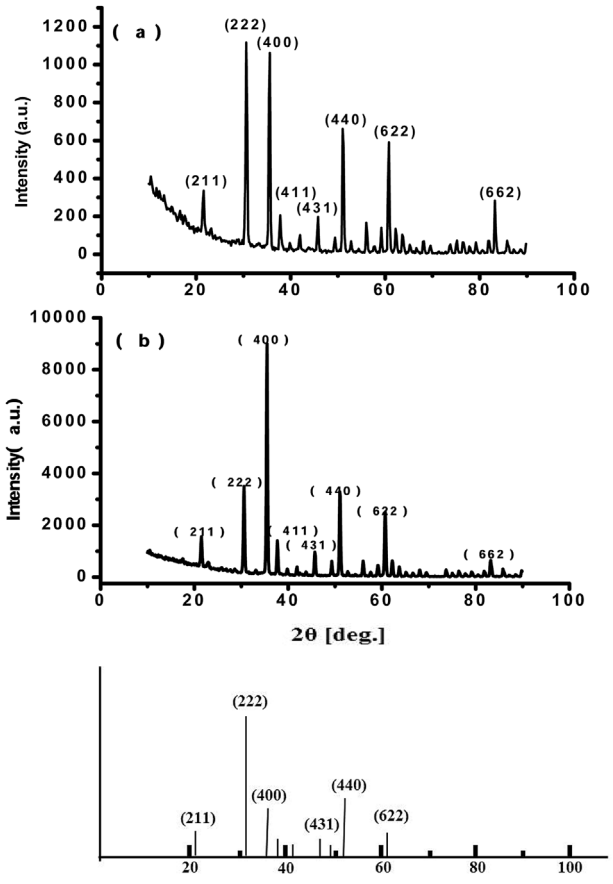

Figure 2 XRD pattern of the obtained products: (a) In_2O_3 microcrystals grown at 900 °C and (b) In_2O_3 micro-rods grown at 1000 °C. The inset of the bottom shows the line spectrum of the bulk In_2O_3 powder (JCPDS No. 89-4595).

which indicates that the percentage of Au in In is below its detection limit by XPS [31].

As for the growth mechanisms of these In_2O_3 microcrystals and In_2O_3 micro-rods, careful observation revealed that a particle-like shape was not found on the top of the structures as it would be in the case of VLS process often reported as the growth mechanism on Au-catalyzed In_2O_3 1D-structures [32–34]. Therefore, the growth mechanism associated with our structures cannot be explained by the well-known VLS mechanism. To elucidate the growth mechanism of In_2O_3 microcrystals and In_2O_3 micro-rods, the structural evolution of these structures was carefully examined step by step during the synthesis process. Figure 4a–d illustrate the typical SEM images of the as-synthesized structures grown at 900 °C for 0, 5, 10, and 20 min when adjusting In metal weight to 0.1 g. The setting growth time of 0 min refers to turning off the furnace immediately after the set temperature of 900 °C is reached. We adopt the VS growth mechanism [35] to explain the formation of the In_2O_3 microcrystals.

At a growth time of 0 min, the growth starts first by the production of In vapor at temperatures above the melting point of In (156–157 °C). The In atoms stick to the Au catalyzed regions and In-rich particles form on the substrate. As $Ar:O_2$ gas mixture is continuously supplied; these particles can agglomerate during temperature increase and form a group of In_2O_3 irregular structures, as shown in Fig. 4a. Indium inside these particles would re-evaporate and will be adsorbed on the structure surface to maintain, together with the incoming adsorbed species from vapor phase, the growth of the structure. As the growth time is increased to 5 min, and while the reaction goes on, the structure provides further preferential accommodation sites for incoming In that may react with oxygen from the argon/oxygen gas mixture source and forms In/In_2O_3 composite at the cone of the structure, as shown in Fig. 4b. Unlike Au during the VLS growth, In/In_2O_3 cone does not form a spherical cap on the top of the structure. It remains faceted suggesting that this composite does not melt. This could result from Au incorporation into In_2O_3 during growth or the Au/In mixture residing at the base of the structure [36, 37].

The growth at this stage can be ascribed to the surface energy of crystallographic planes where preferential adsorption of In/O species on some of these special planes of In_2O_3 takes place, the so-called selective VS growth mechanism. The minimization in surface energy is the main principle in single crystal growth and the crystal morphology evolution is governed by decreasing this energy. Irregular structures shown in Fig. 4a would transform to truncated structures with facets and with base sizes ranging from 650 to 870 nm as illustrated in Fig. 4b. The absence of a particle-like shape on the top of the structure and the occurrence of structure growth only on Au-coated areas suggest that Au catalysts only play a role at the initial stage of the growth. When the growth time is set to 10 min, the In/In_2O_3 composite reaches the saturation concentration and

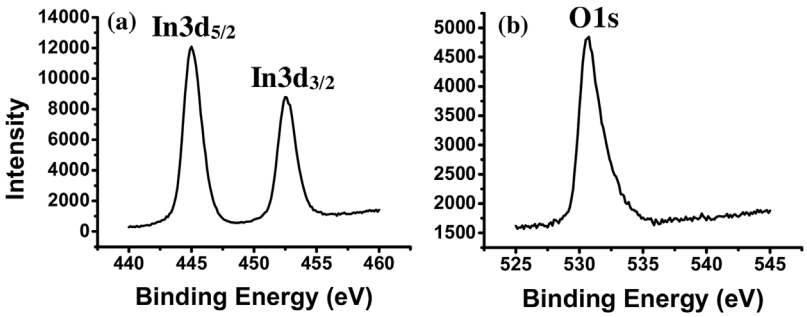

Figure 3 XPS spectra for (a) In3d and (b) oxygen O1s obtained from In_2O_3 microcrystals and In_2O_3 micro-rods.

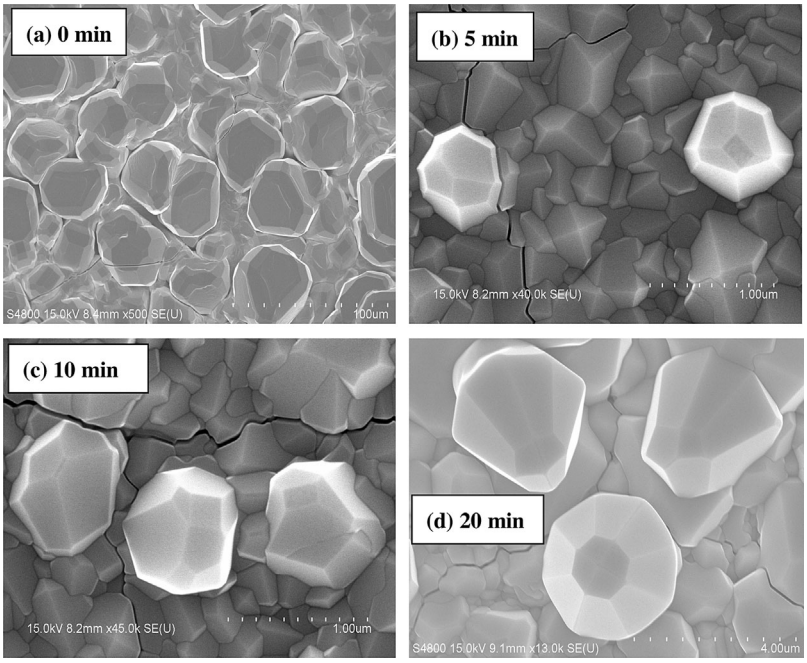

Figure 4 SEM images of as-synthesized In_2O_3 microcrystals at 900 °C and at different growth times of (a) 0 min, (b) 5 min, (c) 10 min, and (d) 20 min.

the growth progresses in a way that reduces the surface energy of the cone and results in the (111) facets at its outmost surfaces. It is known that planes have different growth rates and the ones with slowest growth rate tend to appear as the facets over the other plane. Except for the high energy plane (100), other planes are terminated with the low energy plane (111). The cone is clearly faceted by low-index planes (111) in agreement with previous reports on the growth behavior of In_2O_3 nanostructures suggesting that surface energy of (111) planes is lower than that of other low-index In_2O_3 planes [38, 39]. In_2O_3 planes start to form and appear as facets over the cone's (111) planes. At this stage, structures with base sizes ranging from 650 to 920 nm are obtained as shown in Fig. 4c. As the growth time is increased to 20 min (Fig. 4d), the selective VS growth reaches saturation and the eight facets over the cone planes are found to have the same growth rate resulting in the formation of a full symmetry form of In_2O_3 microcrystal lying over the circular (400) bottom plane. We conclude that the growth of this unique dodecahedron In_2O_3 microcrystal can be attributed to catalyst-assisted selective VS growth and the increase of the growth time has contributed to its high crystallinity.

To elucidate the growth mechanism of In_2O_3 micro-rods, the growth temperature is increased to 1000 °C and the structural evolution of these structures is examined during the synthesis process for different growth times and In metal weights. Figure 5a–d illustrate the typical SEM images of the as-synthesized In_2O_3 micro-rods grown for 25, 30, 40, and 120 min with 0.15, 0.55, 0.7, and 3.8 g of In metal source, respectively.

At higher temperature of 1000 °C, and when the growth time and In weight are increased to 25 min and 0.15 g, respectively, the saturated In_2O_3 microcrystal previously shown in Fig. 4d drives the precipitation of the vapor components of In source material and the oxidized-In at the bottom of the structure as depicted in Fig. 5a. Note that, at this stage, the morphology of the structure has not been affected by varying either the In weight or the growth time. Therefore, both In weight and growth time were varied in experiment II to follow the evolution of the structure. With the increase of In weight to 0.55 g and growth time to 30 min, the adsorbed species would transfer to the (100) plane to maintain the 1D growth along (100) crystalline direction, and as a result, the start of the 1D growth takes place as shown in Fig. 5b. At this stage, In_2O_3 micro-rod with length of about 0.9 μm is obtained. Increasing the In weight to 0.7 and 3.8 g will ensure a continuous supply of vapor components and maintain the 1D growth. As a result, long In_2O_3 micro-rods with length of 1.5 and 8 μm are obtained as shown in Fig. 5c and d. It is found that the diameter of the rod increases slightly toward the bottom (Fig. 5d) from 1.8 μm at the upper part to 2 μm at the bottom. This can be attributed to the exposure of the lower portion of the rod to In vapor for longer time, while the diameter at the most upper part of the rod is confined by the circular bottom plane (100). The results show that the subsequent 1D growth of In_2O_3 rod underneath the In_2O_3 microcrystal can be attributed to self-catalytic VS growth mechanism and the full structure, In_2O_3 micro-rod, can be prepared in a one-step growth synthesis. The increase of growth time has improved the overall crystallinity of these structures.

Compared to other methods being used to synthesize 1D-structures, such as physical vapor deposition (PVD) techniques [40], the Au-catalyzed CVD process utilized in this work is a simpler and cheaper process, and is advantageous for growing In_2O_3 micro-rods/microcrystals

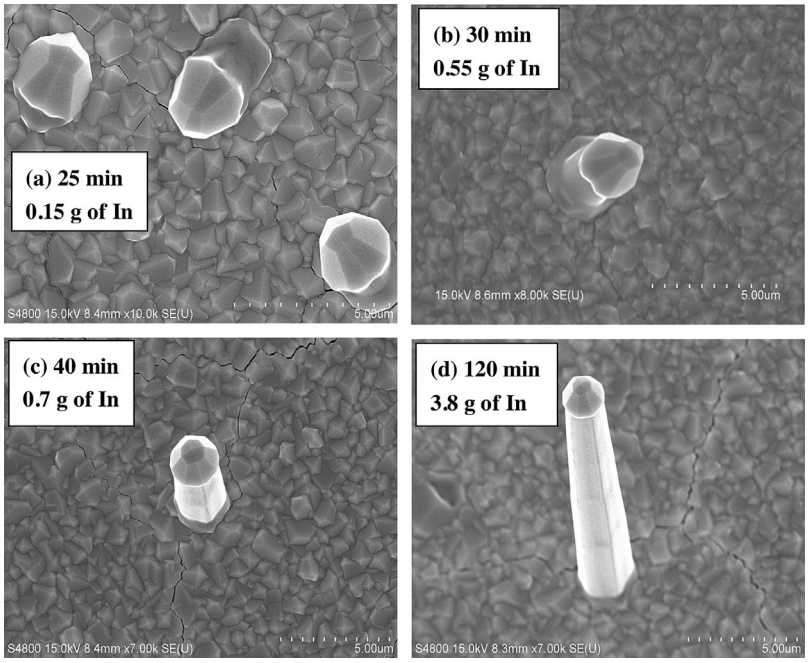

Figure 5 SEM images of as-synthesized In_2O_3 micro-rods at 1000 °C and at different growth times of (a) 25 min, (b) 30 min, (c) 40 min, and (d) 120 min and In metal weights of 0.15, 0.55, 0.7, and 3.8 g, respectively.

with less waste deposition because the growth occurs only on the heated Au-coated surfaces. However, this CVD process runs at much higher temperatures than PVD processes and substrates that cannot tolerate such high growth temperatures must have structures deposited by PVD instead.

Figure 6 shows room temperature PL spectrum of the In_2O_3 micro-rods upon excitation at 260 nm (4.76 eV). The In_2O_3 micro-rods show PL emission at different wavelengths indicating that the PL properties of In_2O_3 material might be affected by its size, dimensionality, and structural shape. This is in agreement with previous reports where PL results exhibited different peaks which may come from the different morphologies. H. Cao et al. observed an ultraviolet (UV) emission at 398 nm in In_2O_3 nanowires embedded in

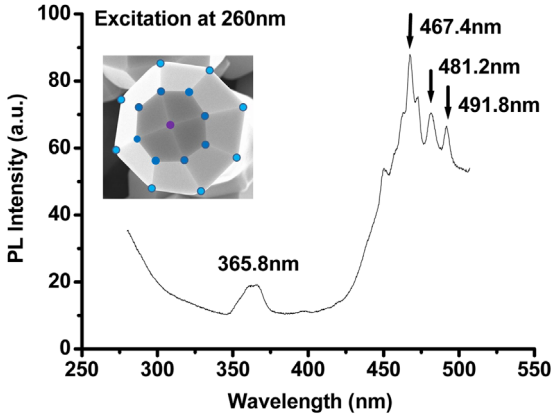

Figure 6 Photoluminescence spectrum from In_2O_3 micro-rods at room temperature upon excitation at 260 nm (4.76 eV); the inset gives close up image of an In_2O_3 microcrystal with marked vertices.

an alumina template [41]; F. Zeng et al. observed two UV emissions at 388 and 401 nm in thermally evaporated In_2O_3 nanowires [42]; An emission in UV centered at 378 nm was also observed by Ching-Jong Chen et al. in In_2O_3 nanowires with hexagonal cross-section [14]. It is well-known that In_2O_3 is an n-type semiconductor with oxygen vacancies acting as the donors. The different amount of oxygen vacancies and defects introduced during the growth process of different In_2O_3 morphologies lead to different transition path of the carriers with new energy states for optical transitions created between the valence and conduction bands. In our case, a luminescence band centered at 365 nm (near UV emission) is observed. This UV PL peak can be attributed to near band edge emission around 3.4 eV from the wide bandgap In_2O_3 micro-rods. The UV transition is believed to be due to the singly ionized oxygen vacancies in the structures, and the emission results from the radiative recombination of a photo-generated hole with an electron occupying this vacancy. More PL emission peaks are observed from this structure covering nearly the whole blue region (450–490 nm) as shown in Fig. 6. A sharp PL emission with its maximum intensity centered at 467 nm (2.65 eV) is detected. Similar peak at 470 nm has been observed in In_2O_3 nanofibers [43]. Because the diameters of our In_2O_3 micro-rods are too large to show a quantum confinement effect, we exclude the possibility of the observed blue PL emission arising from this effect. During our growth experiment, oxygen vacancies might be generated due to rapid evaporation/oxidation process at higher temperature (≥900 °C). Therefore, all of these emission peaks can be referred to trap state emissions, may be due to these oxygen vacancies. The emission would move to a longer wavelength for deeper energy levels, so distinguishable blue light emissions are also observed from

In_2O_3 micro-rods at 481 nm (2.57 eV) and 492 nm (2.52 eV), respectively. Gali et al. have detected similar PL peak at 2.5 eV, which was attributed to the presence of oxygen vacancies created in In_2O_3 nanowires during growth [44]. In our case, the overall UV and blue PL emissions shown in Fig. 6 are from the In_2O_3 micro-rod structure that consists of both an In_2O_3 rod and In_2O_3 microcrystal on top as defined earlier. Some of these PL emissions may come from either In_2O_3 rod or In_2O_3 microcrystal. This can be confirmed in future studies.

Whispering-Gallery mode (WGM) microlasers have attracted great attention as potential light sources for optical interconnection and photonic integrated circuits [45, 46]. The strategy to realize a new and efficient optical resonator becomes the striving direction of many optics researchers. Compared with conventional 1D microcavities, reports on other kind of optical cavities, especially 3D resonators with complex multi-facets are still limited. The inset of Fig. 6 shows the synthesized dodecahedron In_2O_3 microcrystal, which presents many non-parallel facets whose edges intersect each other, creating a high number of vertices. Contrary to the traditional optical cavity in lasers, which consists of a Fabry-Perot (FP) resonator formed by two parallel mirrors and produces a standing-wave pattern within the cavity [47], the advantage of this In_2O_3 dodecahedron is that light can be confined by many boundaries and circulates around due to multiple total internal reflections, exhibiting low loss and high quality factor. Standing-wave pattern in FP resonator often results in wasted energy because of the presence of unexploited gain [48].

Multifaceted optical resonators are potential candidates to overcome this issue due to unidirectional travelling waves that can be obtained, reducing the spatial inhomogeneity in the gain by allowing no standing-wave modes [49]. Furthermore, the In_2O_3 dodecahedron may attract interest for potential application as multiple-port WGM microlaser due to its high number of vertices. Huang et al. [50] have studied the mode characteristics of microresonators with multiple bus waveguides connected to the vertices of the structure and their numerical results of mode Q factors and output coupling efficiencies showed that high efficiency microresonator lasers can be realized. The fabricated dodecahedron In_2O_3 microcrystal may find applications in developing optical devices, especially 3D resonators.

4 Conclusions In summary, In_2O_3 micro-rods are synthesized in an electrical furnace via Au-catalyzed vapor transport process. Each structure consists of an In_2O_3 rod with a unique dodecahedron In_2O_3 microcrystal on top. The growth of the In_2O_3 microcrystal is attributed to catalyst-assisted selective VS growth, while the growth of the In_2O_3 rod underneath the In_2O_3 microcrystal is dominated by the 1D self-catalytic VS growth mechanism. The structural evolution of the products is successfully examined during the synthesis process by controlling the growth parameters. Furthermore, the room-temperature PL spectrum of In_2O_3 micro-rods shows light emission in the UV and blue regions, which may be related to the existence of oxygen vacancies and to the structural shape and morphology of the structure. This work represents an important contribution to understanding and ultimately controlling the growth of these structures. The synthesized dodecahedron In_2O_3 microcrystals contain a large number of vertices and may find many applications in optical devices such as 3D resonators, or other optoelectronic devices, such as UV and blue-light emitters.

Acknowledgement The authors extend their appreciation to the Deanship of Scientific Research at King Saud University for funding this work through research group no IRG14-07A.

References

[1] G. Cheng, E. Stern, S. Guthrie, M. A. Reed, R. Klie, Y. Hao, G. Meng, and L. Zhang, Appl. Phys. A **85**, 233 (2006).
[2] P. Yang, H. Yan, S. Mao, R. Russo, J. Johnson, R. Saykally, N. Morris, J. Pham, R. He, and H. Choi, Adv. Funct. Mater. **12**, 323 (2002).
[3] H. Ouacha, O. Nur, M. Willander, Y. Fu, and A. Ouacha, Appl. Phys. Lett. **69**, 2382 (1996).
[4] Y. Xia, P. Yang, Y. Sun, Y. Wu, B. Mayers, B. Gates, Y. Yin, F. Kim, and H. Yan, Adv. Mater. **15**, 353 (2003).
[5] C. Li, W. Fan, D. A. Straus, B. Lei, S. Asano, D. Zhang, J. Han, M. Meyyappan, and C. Zhou, J. Am. Chem. Soc. **126**, 7750 (2004).
[6] G. Kiriakidis, H. Ouacha, and N. Katsarakis, Nano-structured metal oxide films with room temperature gas sensing properties, edited by T. Tsakalakos, I. A. Ovid'ko, A. K. Vasudevan, in: Nanostructures: Synthesis, Functional Properties and Applications (Kluwer Academic Publishers, Dordrecht, 2003), pp. 363–382.
[7] C. Li, M. Curreli, H. Lin, B. Lei, F. N. Ishikawa, R. Datar, R. J. Cote, M. E. Thompson, and C. Zhou, J. Am. Chem. Soc. **127**, 12484 (2006).
[8] G. Kiriakidis, H. Ouacha, N. Katsarakis, K. Galatsis, and W. Wlodarski, Low Temperature InO_x Thin Films for O_3 and NO_2 Gas Sensing, Proceedings of SPIE: Smart Sensors, Actuators, and MEMS **5116**, 84 (2003).
[9] P. Nguyen, H. T. Ng, T. Yamada, M. K. Smith, J. Li, J. Han, and M. Meyyappan, Nano Lett. **4**, 651 (2004).
[10] G. Kiriakidis, H. Ouacha, and N. Katsarakis, Rev. Adv. Mater. Sci. **4**, 32 (2003).
[11] Q. Wan, M. Wei, D. Zhi, J. L. MacManus-Driscoll, and M. G. Blamire, Adv. Mater. **18**, 234 (2006).
[12] Z. Cheng, X. Dong, Q. Pan, J. Zhang, and X. Dong, Mater. Lett. **60**, 3137 (2006).
[13] H. W. Kim, N. H. Kim, and C. Lee, Appl. Phys. A **81**, 1135 (2005).
[14] C. J. Chen, W. L. Xu, and M. Y. Chern, Adv. Mater. **19**, 3012 (2007).
[15] C. Li, D. Zhang, S. Han, X. Liu, T. Tang, and C. Zhou, Adv. Mater. **15**, 143 (2003).
[16] P. Guha, S. Kar, and S. Chaudhuri, Appl. Phys. Lett. **85**, 3851 (2004).
[17] D. A. Magdas, A. Cremades, and J. Piqueras, Appl. Phys. Lett. **88**, 113107 (2006).
[18] Y. Yan and L. Zhou, Appl. Phys. A **92**, 401 (2008).

[19] C. J. Chen, M. Y. Chern, C. T. Wub, and C. H. Chen, Mater. Res. Bull. **45**, 230 (2010).
[20] A. Qurashi, E. M. El-Maghraby, T. Yamazaki, and T. Kikuta, J. Alloys Comp. **480**, 9 (2009).
[21] O. Bierwagen, Semicond. Sci. Technol. **30**, 024001 (2015).
[22] P. D. C. King, T. D. Veal, F. Fuchs, C. Y. Wang, D. J. Payne, A. Bourlange, H. Zhang, G. R. Bell, V. Cimalla, O. Ambacher, R. G. Egdell, F. Bechstedt, and C. F. McConville, Phys. Rev. B **79**, 205211 (2009).
[23] H. Dong, Y. Liu, S. Sun, Z. Chen, and L. Zhang, J. Mater. Chem. C **2**, 8976–8982 (2014). https://doi.org/10.1039/C4TC01223B
[24] H. Dong, L. Sun, S. Sun, W. Xie, L. Zhou, X. Shen, and Z. Chen, Appl. Phys. Lett. **97**, 223114 (2010).
[25] M. Gulen, G. Yildirim, S. Bal, A. Varilci, I. Belenli, and M. Oz, J. Mater. Sci.: Mater. Electron. **24**, 467–474 (2012). https://doi.org/10.1007/s10854-012-0768-8
[26] Y. Chen, H. Jiang, S. Jiang, X. Liu, W. Zhang, and Q. Zhang, Acta Metall. Sin. (Engl. Lett.) **27**, 368 (2014).
[27] T. Gao and T. Wang, J. Cryst. Growth **290**, 660 (2006).
[28] A. Vomieroa, M. Ferroni, M. M. Natilec, T. Fischere, R. Fize, S. Mathure, and G. Sberveglieri, Appl. Surf. Sci. **323**, 59 (2014).
[29] C. Wang, D. Chen, X. Jiao, and C. Chen, J. Phys. Chem. C **111**, 13398 (2007).
[30] G. Jo, W. K. Hong, J. Maeng, T. W. Kim, G. Wang, A. Yoon, S. S. Kwon, S. Song, and T. Lee, Colloids Surf. A: Physicochem. Eng. Aspects **313-314**, 308 (2008).
[31] A. G. Shard, Surf. Interface Anal. **46**, 175 (2014).
[32] C. J. Chen, W. L. Xu, and M. Y. Chern, Adv. Mater. **19**, 3012 (2007).
[33] B. Wang, Z. Zheng, H. Wu, and L. Zhu, Nanoscale Res. Lett. **9**(111), 1 (2014).
[34] Y. Yan and L. Zhou, Appl. Phys. A **92**, 401 (2008).
[35] M. Y. Yen, C. W. Chiu, C. H. Hsia, F. R. Chen, J. J. Kai, C. Y. Lee, and H. T. Chiu, Adv. Mater. **15**, 235 (2003).
[36] K. Tai, K. Sun, B. Huang, and S. J. Dillon, Nanotechnology **25**, 145603 (2014).
[37] J. M. Lee, F. Xia, W. T. Nichols, C. Choi, and W. I. Park, Met. Mater. Int. **18**, 875 (2012).
[38] K. H. Zhang, A. Walsh, C. R. Catlow, V. K. Lazarov, and R. G. Egdell, Nano Lett. **10**, 3740 (2010).
[39] Y. Hao, G. Meng, C. Ye, and L. Zhang, Cryst. Growth Des. **5**, 1617 (2005).
[40] Y. Zhang, M. K. Ram, E. K. Stefanakos, and D. Y. Goswami, J. Nanomater. **2012**, 1–22 (2012). Article ID 624520, https://doi.org/10.1155/2012/624520
[41] H. Cao, X. Qiu, Y. Liang, Q. Zhu, and M. Zhao, Appl. Phys. Lett. **83**, 761 (2003).
[42] F. Zeng, X. Zhang, J. Wang, L. Wang, and L. Zhang, Nanotechnology **15**, 596 (2004).
[43] C. H. Liang, G. W. Meng, Y. Lei, F. Phillipp, and L. D. Zhang, Adv. Mater. **13**, 1330 (2001).
[44] P. Gali, F. L. Kuo, N. Shepherd, and U. Philipose, Semicond. Sci. Technol. **27**, 015015 (2012).
[45] S. L. McCall, A. F. J. Levi, R. E. Slusher, S. J. Pearton, and R. A. Logan, Appl. Phys. Lett. **60**, 289 (1992).
[46] J. V. Campenhout, P. R. Romeo, P. Regreny, C. Seassal, D. V. Thourhout, S. Verstuyft, L. D. Cioccio, J. M. Fedeli, C. Lagahe, and R. Baets, Opt. Express **15**, 6744 (2007).
[47] A. K. Bhowmik, Appl. Opt. **39**, 3071 (2000).
[48] W. T. Silfvast, Laser Fundamentals (Cambridge University Press, New York, 2008), p. 434.
[49] J. D. Lin, Y. Z. Huang, Y. D. Yang, Q. F. Yao, X. M. Lv, J. L. Xiao, and Y. Du, IEEE Photon. J. **3**, 756 (2011).
[50] Y. Z. Huang, Y. D. Yang, J. D. Lin, K. J. Che, S. J. Wang, J. L. Xiao, and Y. Du, in: Proc. of SPIE on Laser Resonators and Beam Control XIII, San Francisco, USA, 2011 (SPIE, 2011), https://doi.org/10.1117/12.879235